On the Capability of Neural Networks to Generalize to Unseen Category-Pose Combinations

Spandan Madan[†] SEAS, Harvard University
Timothy Henry CBMM & MIT
Jamell Dozier CBMM & MIT
Helen Ho MIT CSAIL

Nishchal Bhandari MIT CSAIL
Tomotake Sasaki Fujitsu Laboratories Ltd.
Frédo Durand MIT CSAIL
Hanspeter Pfister SEAS, Harvard University

Xavier Boix[†] CBMM & MIT

Abstract

Recognizing an object's category and pose lies at the heart of visual understanding. Recent works suggest that deep neural networks (DNNs) often fail to generalize to category-pose combinations not seen during training. However, it is unclear when and how such generalization may be possible. Does the number of combinations seen during training impact generalization? Is it better to learn category and pose in separate networks, or in a single shared network? Furthermore, what are the neural mechanisms that drive the network's generalization? In this paper, we answer these questions by analyzing state-of-the-art DNNs trained to recognize both object category and pose (position, scale, and 3D viewpoint) with quantitative control over the number of category-pose combinations seen during training. We also investigate the emergence of two types of specialized neurons that can explain generalization to unseen combinations—neurons selective to category and invariant to pose, and vice versa. We perform experiments on MNIST extended with position or scale, the iLab dataset with vehicles at different viewpoints, and a challenging new dataset for car model recognition and viewpoint estimation that we introduce in this paper, the *Biased-Cars* dataset. Our results demonstrate that as the number of combinations seen during training increase, networks generalize better to unseen category-pose combinations, facilitated by an increase in the selectivity and invariance of individual neurons. We find that learning category and pose in separate networks compared to a shared one leads to an increase in such selectivity and invariance, as separate networks are not forced to preserve information about both category and pose. This enables separate networks to significantly outperform shared ones at predicting unseen category-pose combinations.

1 Introduction

In recent years, deep neural networks (DNNs) have offered state-of-the-art solutions for object category recognition [1–5], pose estimation (*e.g.,* position, scale, and 3D viewpoint) [6–9], and more complex visual problems that rely on a combination of these two tasks. These include Object Detection [10–16], Visual Question Answering [17–20], and Image Captioning [21–25], among others. Despite this tremendous progress, recent works have uncovered evidence suggesting that generalization capabilities of DNNs might be limited when testing on object category-pose combinations not seen during training. For object category recognition, DNNs may fail to generalize across spatial transformations like 2D rotation and translation [26–28], and also non-canonical 3D views [29, 30].

[†] *Corresponding authors:* spandan_madan@g.harvard.edu and xboix@mit.edu

Ford Thunderbird, Front | Mitsubishi Lancer, Side | Ford Thunderbird, Side

(a)

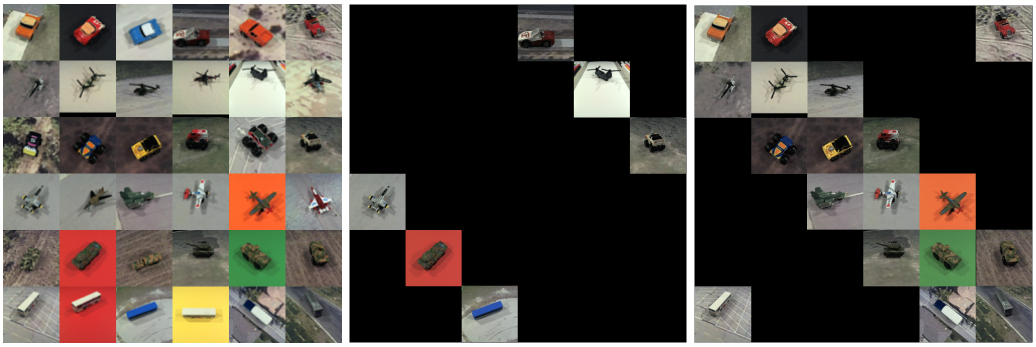

iLab-2M dataset | *Unseen* Combinations (held-out) | 50% *Seen* Combinations

(b) (c) (d)

Figure 1: *Category-Pose datasets.* (a) Our new *Biased-Cars* dataset: Can a network shown only examples of Ford Thunderbird from the front and of Mitsubishi Lancer from the side generalize to predict the Category and the Pose for a Thunderbird seen from the side? (b) iLab-2M dataset [31]: Each cell represents a unique category-pose combination (categories vary between rows, pose between columns) with multiple object instances per category and backgrounds. (c) Held-out test set of category-pose combinations. The same held-out test set is used to evaluate networks trained with different percentage of *seen* combinations. (d) Example of biased training set with 50% of the category-pose combinations. The number of categories and poses selected is always equal.

For pose estimation, DNNs often need to be trained for specific object instances or categories [7–9], which suggests that pose estimation methods do not generalize well across arbitrary 3D objects.

It remains unclear *when* and *how* DNNs generalize across category-pose combinations not seen during training. Fig. 1a presents a motivating example: would a network trained with examples of a Ford Thunderbird seen only from the front, and a Mitsubishi Lancer seen only from the side generalize to predict car model (category) and viewpoint (pose) for a Thunderbird shown from the side? If so, what underlying mechanisms enable a network to do so?

In order to understand the capability of DNNs to generalize to unseen category-pose combinations, we investigate the impact of two key factors—data diversity and architectural choices. More concretely, we train state-of-the-art DNNs on a different number of object category-pose combinations and evaluate them on combinations never seen during training. As category recognition and pose estimation are often needed together to solve complex computer vision tasks, we analyze the impact of learning the two tasks in separate networks *vs.* together on the capability to generalize. Furthermore, to investigate the underlying mechanisms driving the generalization of the network, we investigate the emergence of selective and invariant representations which have been shown to facilitate generalization [32–38].

In a series of experiments, we demonstrate that the percentage of category-pose combinations seen during training (training data diversity) matters significantly. As DNNs are trained with more

combinations, there is an increase in their accuracy on unseen combinations. Our results also reveal that learning category and pose in separate networks helps DNNs generalize substantially better compared to learning them together. We show that this generalization behaviour is driven by an increase in the selectivity and invariance of the neurons, which is even more pronounced when category and pose prediction are learned in separate networks compared to a shared one.

These results are consistent across multiple state-of-the-art DNNs in MNIST [39] extended with position and scale, the iLab-2M dataset [31] and in a new challenging dataset of car model recognition and viewpoint estimation, the *Biased-Cars* dataset, which we introduce in this paper. This new dataset consists of 15K photorealistic rendered images of several car models at different positions, scales and viewpoints, and under various illumination, background, clutter and occlusion conditions. With these results, we hope to provide a first milestone at understanding the neural mechanisms which enable DNNs to generalize to unseen category-pose combinations.

2 Category-Pose Datasets

To analyze generalization to unseen category-pose combinations, we chose the following four datasets as they offer complete control over the joint distribution of categories and poses. Each dataset contains category and pose labels for all images, and networks are trained to predict both these labels simultaneously without pretraining. Category and pose prediction are both cast as classification problems with an equal number of classes to ensure equal treatment of the two tasks. Additional experimental details including optimizers and hyper-parameters can be found in the supplement.

MNIST-Position and MNIST-Scale. These are variants of the MNIST dataset [39], created by adding pose in the form of position or scale to MNIST. MNIST-Position was created by placing MNIST images into one of nine possible locations in an empty 3-by-3 grid. For MNIST-Scale, we resized images to one of nine possible sizes followed by zero-padding. Images of the digit 9 were left out in both these datasets ensuring nine category and nine pose classes, for a total of 81 category-pose combinations. Sample images are available in the supplement.

iLab-2M dataset. iLab-2M [31] is a large scale (two million images), natural image dataset with 3D variations in pose and multiple object instances for each category as shown in Fig.1b. The dataset was created by placing physical toy objects on a turntable and photographing them from six different azimuth viewpoints, each at five different zenith angles (total 30). From the original dataset, we chose a subset of six object categories - Bus, Car, Helicopter, Monster Truck, Plane, and Tank. In Fig. 1b, each row represents images from one category, and each column images from one azimuth angle. All networks are trained to predict one of six category and the azimuth (pose) labels each.

Biased-Cars dataset. Here we introduce a challenging new dataset of object category and pose which we call the *Biased-Cars* dataset. We plan to make it publicly available upon publication. This dataset was generated using our custom computer graphics pipeline to render photo-realistic outdoor scene data with fine control over scene clutter (trees, street furniture, and pedestrians), object occlusions, diverse backgrounds (building/road materials) and lighting conditions (sky maps). Our dataset has 15K images and contains five different car models seen from viewpoints varying between 0-90 degrees of azimuth, and 0-50 degrees of zenith across multiple scales. Sample images are shown in Fig. 1a. For additional diversity, cars were rendered in four different colors—red, green, blue, and black. We divide the azimuth angle into five bins of 18 degrees each, ensuring five category (car models) and five pose classes (azimuth bins), for a total of 25 different category-pose combinations.

Building on the recent successes of synthetic city datasets and simulators for outdoor scenes [40–46], we designed our pipeline for two main reasons. Firstly, existing pre-rendered datasets did not match the experimental constraints we wished to have over the joint distribution of categories, pose, and other scene parameters like object colors, scene clutter, and backgrounds. Secondly, most existing simulators use real-time rendering, and not physically based rendering (PBR) [47]. Using PBR helped make our images more photo-realistic by accurately modeling the flow of light in the scene. Furthermore, PBR has been shown to help networks transfer to natural image data significantly better than real-time rendering [48, 49]. Additional details and samples are available in the supplement.

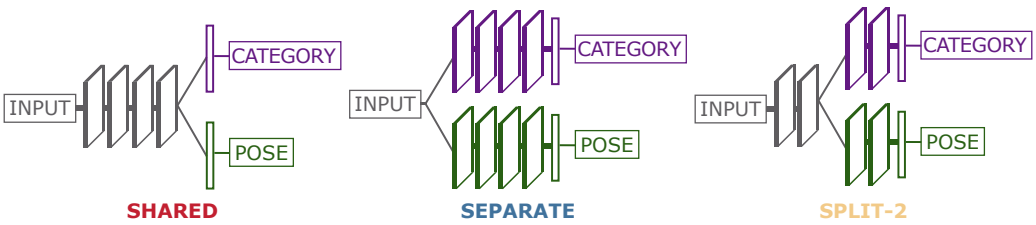

Figure 2: *Architectures for Category Recognition and Pose Estimation. Shared*, *Separate* and *Split-2* architectures for ResNet-18. In the *Shared* architecture, all layers until the last convolutional block are shared between tasks, followed by task specific fully connected layers. In the *Separate* architecture, each task is trained in a separate network with no layer sharing between tasks. *Split-2* presents a middle ground. These architectures are designed similarly for backbones other than ResNet-18.

3 Factors Affecting Generalization to *Unseen* Category-Pose Combinations

Below we present the two factors we study for their impact on generalization to *unseen* category-pose combinations - *(i)* data diversity, and *(ii)* architectural choices.

3.1 Generating Train/Test Splits with Desired Data Diversity

Every dataset described in Section 2 can be visualized as a square category-pose *combinations grid* as shown for the iLab dataset in Fig. 1b. Here, each row represents images from one category, and each column a pose. Thus, each cell in the *combinations grid* represents one category-pose combination.

Constructing the test split. For every dataset, we select and hold out a set of combinations from the *combinations grid* as shown in Fig. 1c. We refer to these as the *unseen* combinations. Images from these combinations are never shown to any network during training. Instead, these images are used to build an *unseen* test split, which allows us to evaluate how well networks generalize to combinations never seen during training. For a fair representation of each category and pose, we ensure that every category and pose class occurs exactly once in the *unseen* combinations, *ie.,* one cell each per row and column is selected. One such *unseen* test split is constructed for each dataset.

Constructing multiple train splits. Remaining cells in the *combinations grid* are used to construct multiple training splits with an increasing percentage of category-pose combinations. For each training split, we first sample a set of combinations as shown in Fig. 1d, which we call the *seen* combinations. Then, we build the training data-split by sampling images from these *seen* combinations. We ensure that every category and pose occurs equally in the *seen* combinations, *ie.,* equal numbers of cells per each row and column. Fig. 1d shows the 50% *seen* training split for the iLab dataset. To ensure that we evaluate the effect of data diversity and not that of the amount of data, the number of images is kept constant across train splits as the percentage of *seen* combinations is increased. Thus, the number of images per *seen* combination decreases as the percentage of *seen* combinations is increased.

3.2 Architectural Choices

One central question addressed in this paper is the impact of architectural choices on the capability to generalize to *unseen* category-pose combinations. Work from Multi-Task Learning [50, 51] literature suggests learning the two tasks in the same network can help generalize better when the tasks are related. However, recent works suggest that architectures composed of specialized networks for sub-tasks [17–19] help improve generalization to novel conditions in relational visual question-answering tasks [52]. To see how this architectural choice impacts generalization to unseen category-pose combinations, we defined two backbone agnostic architectures which we refer to as the *Shared* and the *Separate* architectures. Fig. 2 depicts these architectures for a ResNet-18 backbone [1]. In the *Shared* case, all convolutional blocks are shared between tasks, followed by task-specific fully connected layers, while there are no layers shared between tasks in the *Separate* architecture. Specifically for ResNet-18, we also investigated 3 additional *Split* architectures which represent a gradual transition from *Separate* to *Shared* ResNet-18: the *Split-1*, *Split-2*, and *Split-3* architectures. These were constructed by branching ResNet-18 after 1, 2, and 3 convolutional blocks as compared to after 4 blocks as in the case of the *Shared* architecture as shown in Fig. 2. It is important to note

that splitting a layer leads to the doubling of the number of neurons in that layer. In the experiments below, we show that this increase in width does not provide an added advantage.

4 Generalization through Selectivity and Invariance of Individual Neurons

Selectivity and invariance of neurons have long been hypothesized to facilitate generalization in both biological and artificial neural networks [33–36, 38, 53–55]. Neurons are commonly interpreted as image feature detectors, such that the neuron's activity is high only when certain features are present in the image [56–60]. We refer to this property as *selectivity* to an image feature. Selectivity alone, however, is not sufficient to generalize to *unseen* category-pose combinations. For example, a neuron may be selective to features relevant to a category, but only so for a subset of all the poses. Generalization is facilitated by selective neurons that are also *invariant* to nuisance features. For instance, in Fig. 1a, neurons that are selective to the Ford Thunderbird and invariant to pose would have very similar activity for the Ford Thunderbird in *seen* and *unseen* poses, thus enabling generalization to category recognition. Similarly, generalization to pose prediction can be enabled by neurons selective to pose and invariant to category.

Here, we present our implementation for quantifying the amount of *selectivity* and *invariance* of an individual neuron. Let N be the number of categories or poses in the dataset. We represent the activations for a neuron across all category-pose combinations as an $N \times N$ *activations grid*, as shown in Fig. E.16a. Each cell in this *activations grid* represents the average activation of a neuron for images from one category-pose combination, with rows and columns representing average activations for all images from a single category (*e.g.,* Ford Thunderbird) and a pose (*e.g.,* front), respectively. These activations are normalized to lie between 0 and 1 (see supplement). For neuron k, we define a^k_{ij} as the entry in the *activations grid* for column (category) i and row (pose) j. Below we introduce the evaluation of a neuron's *selectivity score* with respect to category and *invariance score* with respect to pose. Pose selectivity score and category invariance score can be derived analogously.

Selectivity score. We first identify the category that the neuron is activated for the most on average, *ie.,* the category which has the maximum sum across the column in Fig. E.16a. We call this category the neuron's *preferred category*, and denote it as $i^{\star k}$, such that $i^{\star k} = \arg\max_i \sum_j a^k_{ij}$. The selectivity score compares the average activity for the *preferred category* (denoted as $\hat{a}^k$) with the average activity of the remaining categories ($\bar{a}^k$). Let S^k_c be the selectivity score with respect to category, which we define as is usual in the literature (*e.g.,* [61, 62]) with the following expression:

$$S^k_c = \frac{\hat{a}^k - \bar{a}^k}{\hat{a}^k + \bar{a}^k}, \quad \text{where } \hat{a}^k = \frac{1}{N}\sum_j a^k_{i^{\star k}j}, \;\; \bar{a}^k = \frac{\sum_{i \neq i^{\star k}} \sum_j a^k_{ij}}{N(N-1)}. \tag{1}$$

Observe that S^k_c is a value between 0 and 1, and higher values of S^k_c indicate that the neuron is more active for the *preferred category* as compared to the rest. Selectivity with respect to pose, denoted as S^k_p, can be derived analogously by swapping indices (i, j).

Invariance score. A neuron's invariance to pose captures the range of its average activity for the *preferred category* as the pose (nuisance parameter) is changed. Let I^k_p be the invariance score with respect to pose which we define as the difference between the highest and lowest activity across all poses for the *preferred category*, *ie.,*

$$I^k_p = 1 - \Big(\max_j \;\; a^k_{i^{\star k}j} - \min_j \;\; a^k_{i^{\star k}j}\Big), \tag{2}$$

where the range is subtracted from 1 to have the invariance score equal to 1 when there is maximal invariance. Invariance with respect to category, denoted I^k_c, can be derived analogously.

Specialization score. Generalization to category recognition may be facilitated by neurons selective to category and invariant to pose. Similarly, pose selective and category invariant neurons can help generalize well to pose estimation. This reveals a tension when category and pose are learned together, as a neuron which is selective to category, cannot be invariant to category. The same is true for pose. One way to resolve this contradiction is the emergence of two sets of *specialized* neurons - category selective and pose invariant, and vice versa. This hypothesis is well-aligned with the findings in [63], which showed the emergence of groups of neurons contributing exclusively to single tasks. Thus, in the context of category recognition and pose estimation, we hypothesize that neurons become selective to either category or pose as the relevant image features for these tasks are disjoint.

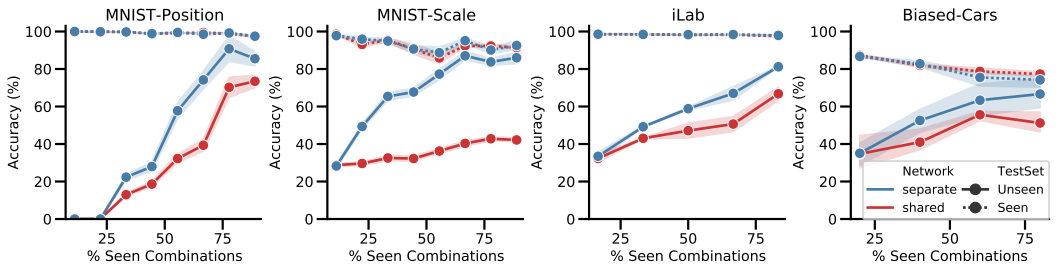

Figure 3: *Generalization performance for Shared and Separate ResNet-18 as seen combinations are increased for all datasets.* The geometric mean between category recognition accuracy and pose estimation accuracy is reported along with confidence intervals (a) MNIST-Scale dataset. (b) MNIST-Position dataset. (c) iLab dataset. (d) Biased-Cars dataset.

To classify neuron k as a category or pose neuron, we compare its selectivity for both category and pose (S_c^k and S_p^k). If S_c^k is greater than S_p^k, then neuron k is a category neuron, otherwise, it is a pose neuron. Since generalization capability relies on both invariance and selectivity, we introduce a new metric for a neuron, the *specialization score* denoted as Γ^k, which is the geometric mean of its selectivity and invariance scores, *ie.,*

$$\Gamma^k = \begin{cases} \sqrt{S_c^k I_p^k} & \text{if } S_c^k > S_p^k \quad \text{(category neuron)} \\ \sqrt{S_p^k I_c^k} & \text{if } S_c^k \leq S_p^k \quad \text{(pose neuron)} \end{cases} . \tag{3}$$

In Section 6 we present results that show that the *specialization score* is highly indicative of a network's capability to generalize to *unseen* combinations.

5 When do DNNs Generalize to new Category-Pose Combinations?

Below we summarize our findings from evaluating *Separate* and *Shared* architectures when tested on images from *seen* (different from train images) and *unseen* category-pose combinations. See supplement for experimental details.

DNNs generalize better to *unseen* combinations as they see more combinations. Fig. 3 presents the geometric mean of category and pose prediction accuracy for *Separate* and *Shared* architectures with the ResNet-18 backbone, for all datasets. These experiments were repeated three times, and here we present the mean performance with confidence intervals. As Fig. 3 shows, both architectures show a significant improvement in their performance on images from *unseen* combinations, as the *seen* combinations are increased. Thus, an increase in data diversity in the form of *seen* combinations enables both these architectures to generalize better. It is to be noted that state-of-the-art DNNs do not theoretically guarantee viewpoint invariance [38]. But this result provides reassurance that DNNs can become robust to unseen category-pose combinations as long as they are shown enough diversity during training. However, the accuracy for both category and pose prediction may not always be increasing consistently (see supplement), even though their geometric mean (shown above) is always increasing. We attribute this to the randomness in the selection of *seen* and *unseen* combinations.

***Separate* architectures generalize significantly better than *Shared* ones.** A striking finding that emerged from our analysis is that while both architectures perform well on new images from *seen* combinations, for images from *unseen* combinations *Separate* architectures outperform *Shared* ones by a very large margin. For the ResNet-18 backbone, this result can be seen consistently across all 4 datasets as shown in Fig. 3. Results for each individual task have been shown in the supplement.

We extended our analysis to *Separate* and *Shared* architectures with different backbones (ResNeXt [2], WideResNet [3], Inception v3 [4] and the DenseNet [5]), as shown in Fig. 4a and b. As can be seen, *Separate* architectures outperform *Shared* ones by a large margin for all backbones, which confirms that this result is not backbone specific. Investigating further, we experiment with *Split* architectures, and as can be seen in Fig. 4c and d, there is a consistent, gradual dip in the performance as we move from the *Separate* to the *Shared* architectures. Thus, generalization to *unseen* category-

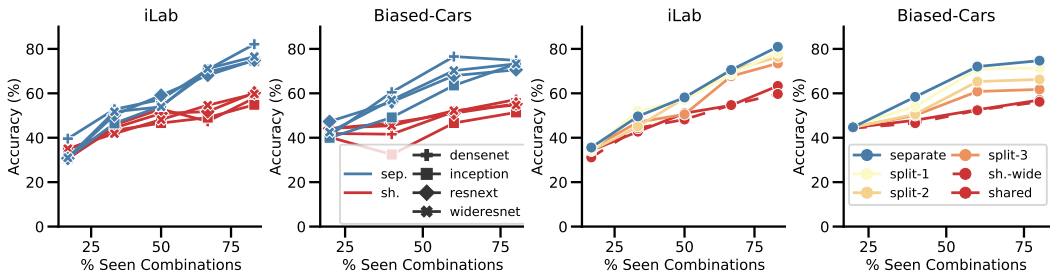

Figure 4: *Generalization performance for different architectures and backbones as seen combinations are increased for all iLab and Biased-City datasets.* The geometric mean between category recognition accuracy and pose recognition accuracy is reported for *unseen* combinations as percentage of *seen* combinations is increased. (a) and (b) Accuracy of *separate* and *shared* for backbones other than ResNet-18, for iLab and Biased-Cars datasets, respectively. (c) and (d) Accuracy of ResNet-18 *Separate*, *Shared* and different *Split* architectures made at different blocks of the network, for iLab and Biased-Cars datasets, respectively.

pose combinations is best achieved by learning both tasks separately, with a consistent decrease in generalization as more parameter sharing is enforced.

To make sure that *Separate* architectures do not perform better due to the added number of neurons, we made the *Shared-Wide* architecture by doubling the neurons in each layer of the *Shared* ResNet-18 network. As Fig. 4c and d show, this architecture performs very similarly to the *Shared* one. This is in accordance with previous results that show that modern DNNs may improve in performance as the width is increased but to a limited extent [64, 65]. See additional results in supplement along with results demonstrating that these findings are robust for a different number of training images.

6 How do DNNs Generalize to Unseen Category-Pose Combinations?

We now analyze the role of specialized (*ie.,* selective and invariant) neurons in driving generalization to *unseen* category-pose combinations presented in Section 5.

Specialization score correlates with generalization to *unseen* category-pose. We first investigate the emergence of category and pose neurons in the final convolutional layer of the networks. Fig. 5b and c show the percentage of neurons of each type in *Shared* and *Separate* architectures as *seen* combinations are increased. As can be seen, all neurons in the category and pose branches of the *Separate* architecture become specialized to category and pose respectively. But in the *Shared* case, as the network is expected to simultaneously learn both tasks, both kinds of neurons emerge. In Fig. E.16 we present the median of specialization scores across neurons, *ie.,* the median of Γ^k, in the final convolutional layer for *Shared*, *Split*, and *Separate* architectures across multiple backbones in *Biased-Cars* dataset. These are presented separately for the category and pose neurons. We show that as *seen* combinations increase, there is a steady increase in the specialization score for both category and pose neurons, suggesting specialization. These trends mirror the generalization trends for networks which suggests that specialization facilitates generalization to *unseen* combinations. In the supplement, we present these results for the other datasets, which support the same conclusions. Also, we show that as expected, the specialization builds up across layers [35, 38].

***Separate* networks facilitate the emergence of specialized neurons.** Fig. E.16 reveals that *Separate* architectures facilitate specialization, while the *Shared* architecture makes it harder for the neurons to specialize (lower specialization scores). This might be because the *Shared* architecture tries to split into two specialized parts, but this specialization is much stronger in the *Separate* architecture due to already having separate branches. This capability to specialize could explain why the *Separate* architecture generalizes better to *unseen* category-pose combinations.

Limitations. In this paper, we have considered selectivity and invariance of individual neurons as a model for understanding generalization to *unseen* combinations. This model is limited in several ways as it only considers the properties of individual neurons, and assumes that selectivity to one single

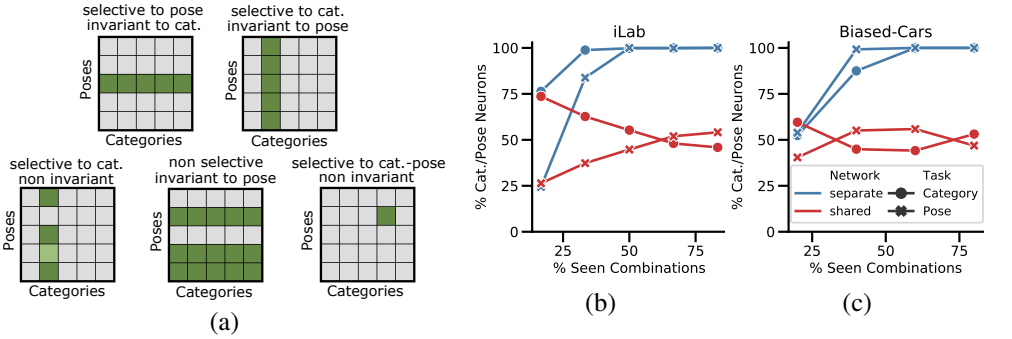

Figure 5: *Specialization to category recognition and pose estimation.* (a) Prototypical *activation grids* for different types of selective and invariant neurons. (b) and (c) Percentage of neurons after ResNet-18 block-4 that are specialized to category and pose, for iLab and Biased-Cars datasets, respectively. ResNet-18 *Separate* and *Shared* networks are evaluated; for *Separate*, only the task-relevant neurons for each branch are displayed.

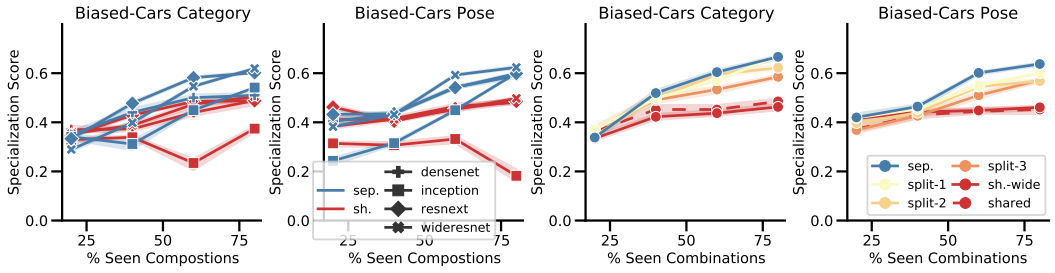

Figure 6: *Neuron specialization (selectivity to category and invariance to pose, and vice versa) in the Biased-Cars dataset.* (a) and (b) Median of the specialization score among neurons (Γ^k) in network architectures, other than ResNet-18, *separate* and *shared*, for category and pose recognition tasks, respectively. Confidence intervals displayed in low opacity. (c) and (d) Median of the specialization score among neurons in ResNet-18 *Separate* and *Shared* with splits made at different blocks of the network, for category and pose recognition tasks, respectively.

category (or pose) is needed alongside invariance to pose (or category) to achieve generalization. There could be other ways to achieve generalization not taken into account by the model. Also, the evidence presented here is correlational and based on the average neural activity for a set of images. Nonetheless, the model has been shown to be useful to explain in simple and intuitive terms why the *Separate* architecture outperforms the *Shared* one, and how these generalize as more category-pose combinations are seen.

7 Conclusions and Future Work

In this paper, we have demonstrated extensively that DNNs generalize better to unseen category-pose combinations as the training data diversity grows. We have also shown that networks trained separately for category recognition and pose estimation surpass a shared network learning both tasks by a large margin when tested on such unseen combinations. We attribute this to the fact that branches in the *Separate* architecture are not forced to preserve information about both category and pose, which facilitates an increase in the selectivity and invariance at the individual neuronal level. Our results were consistent across five different state-of-the-art DNN backbones and four datasets, one of them introduced in this paper to evaluate the ability of the networks to recognize novel combinations of car models and viewpoints in a controlled yet photo-realistic dataset.

These results add to the growing body of works that introduce controlled experiments to understand the generalization abilities of DNNs, *e.g.,* [30, 66]. We hope that this paper serves as a basis for further explorations, as we have left several key questions that need to be resolved in future works. These include understanding the impact of having a larger number of tasks, multiple objects in the

image, and non-uniform ways of holing-out the test set across tasks, among others. We are also intrigued to find out which other factors can lead to an increase in selective and invariant neural representations, as this can help improve the generalization behaviour of computer vision applications.

Statement of Broader Impact

Many practical applications of deep networks require the ability to robustly extrapolate to novel data beyond the training set. With the prevalence of DNNs increasing at an unprecedented rate, understanding the capabilities and limitations of DNNs to generalize is of paramount importance. With this work, we hope to have contributed to the use of deep networks in our society positively in three concrete ways. Firstly, our findings can reassure practitioners that DNNs can generalize to unseen category-pose combinations, as long as enough data diversity is ensured in the training dataset. Secondly, these results can help practitioners make informed architectural choices, helping them build networks that may extrapolate to unseen situations more robustly. Finally, we put forth a simple model for understanding the underlying mechanisms driving the generalization of DNNs at the individual neuron level.

Acknowledgments and Disclosure of Funding

We are grateful to Tomaso Poggio for his insightful advice and warm encouragement. This work has been partially supported by NSF grant IIS-1901030, a Google Faculty Research Award, the Toyota Research Institute, the Center for Brains, Minds and Machines (funded by NSF STC award CCF-1231216), Fujitsu Laboratories Ltd. (Contract No. 40008819) and the MIT-Sensetime Alliance on Artificial Intelligence. We also thank Kumaraditya Gupta for help with the figures, and Prafull Sharma for insightful discussions.

References

[1] Kaiming He, Xiangyu Zhang, Shaoqing Ren, and Jian Sun. Deep residual learning for image recognition. In *Proceedings of the IEEE Conference on Computer Vision and Pattern Recognition (CVPR)*, pages 770–778, 2016.

[2] Saining Xie, Ross Girshick, Piotr Dollár, Zhuowen Tu, and Kaiming He. Aggregated residual transformations for deep neural networks. In *Proceedings of the IEEE Conference on Computer Vision and Pattern Recognition (CVPR)*, pages 1492–1500, 2017.

[3] Sergey Zagoruyko and Nikos Komodakis. Wide residual networks. In *Proceedings of the British Machine Vision Conference (BMVC)*, pages 87.1–87.12, 2016.

[4] Christian Szegedy, Vincent Vanhoucke, Sergey Ioffe, Jon Shlens, and Zbigniew Wojna. Rethinking the inception architecture for computer vision. In *Proceedings of the IEEE Conference on Computer Vision and Pattern Recognition (CVPR)*, pages 2818–2826, 2016.

[5] Gao Huang, Zhuang Liu, Laurens Van Der Maaten, and Kilian Q Weinberger. Densely connected convolutional networks. In *Proceedings of the IEEE Conference on Computer Vision and Pattern Recognition (CVPR)*, pages 4700–4708, 2017.

[6] Weicheng Kuo, Bharath Hariharan, and Jitendra Malik. Deepbox: Learning objectness with convolutional networks. In *Proceedings of the IEEE International Conference on Computer Vision (ICCV)*, pages 2479–2487, 2015.

[7] Yaming Wang, Xiao Tan, Yi Yang, Xiao Liu, Errui Ding, Feng Zhou, and Larry S Davis. 3D pose estimation for fine-grained object categories. In *Proceedings of the European Conference on Computer Vision (ECCV) Workshop*, pages 619–632, 2018.

[8] Chen Wang, Danfei Xu, Yuke Zhu, Roberto Martín-Martín, Cewu Lu, Li Fei-Fei, and Silvio Savarese. DenseFusion: 6D object pose estimation by iterative dense fusion. In *Proceedings of the IEEE Conference on Computer Vision and Pattern Recognition (CVPR)*, pages 3343–3352, 2019.

[9] Yang Xiao, Xuchong Qiu, Pierre-Alain Langlois, Mathieu Aubry, and Renaud Marlet. Pose from shape: Deep pose estimation for arbitrary 3D objects. In *Proceedings of the British Machine Vision Conference (BMVC)*, 2019.

[10] Jifeng Dai, Yi Li, Kaiming He, and Jian Sun. R-FCN: Object detection via region-based fully convolutional networks. In *Advances in Neural Information Processing Systems*, pages 379–387, 2016.

[11] Joseph Redmon and Ali Farhadi. YOLO9000: better, faster, stronger. In *Proceedings of the IEEE Conference on Computer Vision and Pattern Recognition (CVPR)*, pages 7263–7271, 2017.

[12] Cheng-Yang Fu, Wei Liu, Ananth Ranga, Ambrish Tyagi, and Alexander C Berg. DSSD: Deconvolutional single shot detector. *arXiv preprint arXiv:1701.06659*, 2017.

[13] Li Liu, Wanli Ouyang, Xiaogang Wang, Paul Fieguth, Jie Chen, Xinwang Liu, and Matti Pietikäinen. Deep learning for generic object detection: A survey. *International Journal of Computer Vision*, 128(2):261–318, 2020.

[14] Xiongwei Wu, Doyen Sahoo, and Steven CH Hoi. Recent advances in deep learning for object detection. *Neurocomputing*, 2020.

[15] Jiaping Zhao, Chin-kai Chang, and Laurent Itti. Learning to recognize objects by retaining other factors of variation. In *Proceedings of the IEEE Winter Conference on Applications of Computer Vision (WACV)*, pages 560–568. IEEE, 2017.

[16] Asako Kanezaki, Yasuyuki Matsushita, and Yoshifumi Nishida. RotationNet for joint object categorization and unsupervised pose estimation from multi-view images. *IEEE Transactions on Pattern Analysis and Machine Intelligence*, 2019.

[17] Jacob Andreas, Marcus Rohrbach, Trevor Darrell, and Dan Klein. Neural module networks. In *Proceedings of the IEEE Conference on Computer Vision and Pattern Recognition (CVPR)*, pages 39–48, 2016.

[18] Ronghang Hu, Jacob Andreas, Marcus Rohrbach, Trevor Darrell, and Kate Saenko. Learning to reason: End-to-end module networks for visual question answering. In *Proceedings of the IEEE International Conference on Computer Vision (ICCV)*, pages 804–813, 2017.

[19] Justin Johnson, Bharath Hariharan, Laurens Van Der Maaten, Judy Hoffman, Li Fei-Fei, C Lawrence Zitnick, and Ross Girshick. Inferring and executing programs for visual reasoning. In *Proceedings of the IEEE International Conference on Computer Vision (ICCV)*, pages 2989–2998, 2017.

[20] Seung Wook Kim, Makarand Tapaswi, and Sanja Fidler. Visual reasoning by progressive module networks. In *Proceedings of the International Conference on Learning Representations (ICLR)*, 2019.

[21] Jeffrey Donahue, Lisa Anne Hendricks, Sergio Guadarrama, Marcus Rohrbach, Subhashini Venugopalan, Kate Saenko, and Trevor Darrell. Long-term recurrent convolutional networks for visual recognition and description. In *The IEEE Conference on Computer Vision and Pattern Recognition (CVPR)*, 2015.

[22] Marco Pedersoli, Thomas Lucas, Cordelia Schmid, and Jakob Verbeek. Areas of attention for image captioning. In *Proceedings of the IEEE International Conference on Computer Vision (ICCV)*, pages 1242–1250, 2017.

[23] Jiasen Lu, Caiming Xiong, Devi Parikh, and Richard Socher. Knowing when to look: Adaptive attention via a visual sentinel for image captioning. In *Proceedings of the IEEE Conference on Computer Vision and Pattern Recognition (CVPR)*, pages 375–383, 2017.

[24] Yufei Wang, Zhe Lin, Xiaohui Shen, Scott Cohen, and Garrison W Cottrell. Skeleton key: Image captioning by skeleton-attribute decomposition. In *Proceedings of the IEEE Conference on Computer Vision and Pattern Recognition (CVPR)*, pages 7272–7281, 2017.

[25] Xu Yang, Hanwang Zhang, and Jianfei Cai. Learning to collocate neural modules for image captioning. In *Proceedings of the IEEE International Conference on Computer Vision (ICCV)*, pages 4250–4260, 2019.

[26] Logan Engstrom, Brandon Tran, Dimitris Tsipras, Ludwig Schmidt, and Aleksander Madry. Exploring the landscape of spatial robustness. In *Proceedings of the International Conference on Machine Learning (ICML)*, pages 1802–1811, 2019.

[27] Aharon Azulay and Yair Weiss. Why do deep convolutional networks generalize so poorly to small image transformations? *Journal of Machine Learning Research*, 20(184):1–25, 2019.

[28] Sanjana Srivastava, Guy Ben-Yosef, and Xavier Boix. Minimal images in deep neural networks: Fragile object recognition in natural images. In *Proceedings of the International Conference on Learning Representations (ICLR)*, 2019.

[29] Michael A Alcorn, Qi Li, Zhitao Gong, Chengfei Wang, Long Mai, Wei-Shinn Ku, and Anh Nguyen. Strike (with) a pose: Neural networks are easily fooled by strange poses of familiar objects. In *Proceedings of the IEEE Conference on Computer Vision and Pattern Recognition (CVPR)*, pages 4845–4854, 2019.

[30] Andrei Barbu, David Mayo, Julian Alverio, William Luo, Christopher Wang, Dan Gutfreund, Josh Tenenbaum, and Boris Katz. ObjectNet: A large-scale bias-controlled dataset for pushing the limits of object recognition models. In *Advances in Neural Information Processing Systems*, pages 9448–9458, 2019.

[31] Ali Borji, Saeed Izadi, and Laurent Itti. iLab-20M: A large-scale controlled object dataset to investigate deep learning. In *Proceedings of the IEEE Conference on Computer Vision and Pattern Recognition (CVPR)*, pages 2221–2230, 2016. The dataset is available at `https://bmobear.github.io/projects/viva/`.

[32] C Lee Giles and Tom Maxwell. Learning, invariance, and generalization in high-order neural networks. *Applied Optics*, 26(23):4972–4978, 1987.

[33] Emanuela Bricolo, Tomaso Poggio, and Nikos K Logothetis. 3D object recognition: A model of view-tuned neurons. In *Advances in Neural Information Processing Systems*, pages 41–47, 1997.

[34] Maximilian Riesenhuber and Tomaso Poggio. Just one view: Invariances in inferotemporal cell tuning. In *Advances in Neural Information Processing Systems*, pages 215–221, 1998.

[35] Ian Goodfellow, Honglak Lee, Quoc V Le, Andrew Saxe, and Andrew Y Ng. Measuring invariances in deep networks. In *Advances in Neural Information Processing Systems*, pages 646–654, 2009.

[36] Jure Sokolic, Raja Giryes, Guillermo Sapiro, and Miguel Rodrigues. Generalization error of invariant classifiers. In *Proceedings of the International Conference on Artifi-cial Intelligence and Statistics (AISTATS)*, pages 1094–1103, 2017.

[37] Alessandro Achille and Stefano Soatto. Emergence of invariance and disentanglement in deep representations. *The Journal of Machine Learning Research*, 19(1):1947–1980, 2018.

[38] Tomaso Poggio and Fabio Anselmi. *Visual cortex and deep networks: learning invariant representations*. MIT Press, 2016.

[39] Yann LeCun, Léon Bottou, Yoshua Bengio, and Patrick Haffner. Gradient-based learning applied to document recognition. *Proceedings of the IEEE*, 86(11):2278–2324, 1998. The dataset is available at `http://yann.lecun.com/exdb/mnist/`.

[40] Weichao Qiu and Alan Yuille. UnrealCV: Connecting computer vision to Unreal Engine. In *Proceedings of the European Conference on Computer Vision (ECCV)*, pages 909–916, 2016.

[41] Holger Caesar, Varun Bankiti, Alex H Lang, Sourabh Vora, Venice Erin Liong, Qiang Xu, Anush Krishnan, Yu Pan, Giancarlo Baldan, and Oscar Beijbom. nuScenes: A multimodal dataset for autonomous driving. *arXiv preprint arXiv:1903.11027*, 2019.

[42] Alexey Dosovitskiy, German Ros, Felipe Codevilla, Antonio Lopez, and Vladlen Koltun. CARLA: An open urban driving simulator. In *Proceedings of the Annual Conference on Robot Learning (CoRL)*, pages 1–16, 2017.

[43] Rawal Khirodkar, Donghyun Yoo, and Kris Kitani. Domain randomization for scene-specific car detection and pose estimation. In *2019 IEEE Winter Conference on Applications of Computer Vision (WACV)*, pages 1932–1940. IEEE, 2019.

[44] Aayush Prakash, Shaad Boochoon, Mark Brophy, David Acuna, Eric Cameracci, Gavriel State, Omer Shapira, and Stan Birchfield. Structured domain randomization: Bridging the reality gap by context-aware synthetic data. In *Proceedings of the International Conference on Robotics and Automation (ICRA)*, pages 7249–7255. IEEE, 2019.

[45] Yohann Cabon, Naila Murray, and Martin Humenberger. Virtual KITTI 2. *arXiv preprint arXiv:2001.10773*, 2020.

[46] Adrien Gaidon, Qiao Wang, Yohann Cabon, and Eleonora Vig. Virtual worlds as proxy for multi-object tracking analysis. In *Proceedings of the IEEE Conference on Computer Vision and Pattern Recognition (CVPR)*, pages 4340–4349, 2016.

[47] Matt Pharr, Wenzel Jakob, and Greg Humphreys. *Physically based rendering: From theory to implementation*. Morgan Kaufmann, 2016.

[48] Yinda Zhang, Shuran Song, Ersin Yumer, Manolis Savva, Joon-Young Lee, Hailin Jin, and Thomas Funkhouser. Physically-based rendering for indoor scene understanding using convolutional neural networks. In *Proceedings of the IEEE Conference on Computer Vision and Pattern Recognition (CVPR)*, pages 5287–5295, 2017.

[49] Shirsendu Sukanta Halder, Jean-François Lalonde, and Raoul de Charette. Physics-based rendering for improving robustness to rain. In *Proceedings of the IEEE International Conference on Computer Vision (CVPR)*, pages 10203–10212, 2019.

[50] Rich Caruana. Multitask learning. *Machine learning*, 28(1):41–75, 1997.

[51] Trapit Bansal, Arvind Neelakantan, and Andrew McCallum. RelNet: End-to-end modeling of entities & relations. *arXiv preprint arXiv:1706.07179*, 2017.

[52] Dzmitry Bahdanau, Shikhar Murty, Michael Noukhovitch, Thien Huu Nguyen, Harm de Vries, and Aaron Courville. Systematic generalization: What is required and can it be learned? In *Proceedings of the International Conference on Learning Representations (ICLR)*, 2019.

[53] Bruno A Olshausen, Charles H Anderson, and David C Van Essen. A neurobiological model of visual attention and invariant pattern recognition based on dynamic routing of information. *Journal of Neuroscience*, 13(11):4700–4719, 1993.

[54] R Quian Quiroga, Leila Reddy, Gabriel Kreiman, Christof Koch, and Itzhak Fried. Invariant visual representation by single neurons in the human brain. *Nature*, 435(7045):1102–1107, 2005.

[55] Nicole C Rust and James J DiCarlo. Selectivity and tolerance ("invariance") both increase as visual information propagates from cortical area V4 to IT. *Journal of Neuroscience*, 30(39): 12978–12995, 2010.

[56] Matthew D Zeiler and Rob Fergus. Visualizing and understanding convolutional networks. In *European conference on computer vision*, pages 818–833. Springer, 2014.

[57] Karen Simonyan, Andrea Vedaldi, and Andrew Zisserman. Deep inside convolutional networks: Visualising image classification models and saliency maps. *arXiv preprint arXiv:1312.6034*, 2013.

[58] Bolei Zhou, Aditya Khosla, Agata Lapedriza, Aude Oliva, and Antonio Torralba. Object detectors emerge in deep scene cnns. In *Proceedings of the International Conference on Learning Representations (ICLR)*, 2015.

[59] David Bau, Bolei Zhou, Aditya Khosla, Aude Oliva, and Antonio Torralba. Network dissection: Quantifying interpretability of deep visual representations. In *Proceedings of the IEEE Conference on Computer Vision and Pattern Recognition (CVPR)*, pages 6541–6549, 2017.

[60] Maxime Oquab, Léon Bottou, Ivan Laptev, and Josef Sivic. Is object localization for free?-weakly-supervised learning with convolutional neural networks. In *Proceedings of the IEEE Conference on Computer Vision and Pattern Recognition (CVPR)*, pages 685–694, 2015.

[61] Ari S Morcos, David GT Barrett, Neil C Rabinowitz, and Matthew Botvinick. On the importance of single directions for generalization. In *Proceedings of the International Conference on Learning Representations (ICLR)*, 2018.

[62] Bolei Zhou, Yiyou Sun, David Bau, and Antonio Torralba. Revisiting the importance of individual units in cnns via ablation. *arXiv preprint arXiv:1806.02891*, 2018.

[63] Guangyu Robert Yang, Madhura R Joglekar, H Francis Song, William T Newsome, and Xiao-Jing Wang. Task representations in neural networks trained to perform many cognitive tasks. *Nature Neuroscience*, 22(2):297–306, 2019.

[64] Preetum Nakkiran, Gal Kaplun, Yamini Bansal, Tristan Yang, Boaz Barak, and Ilya Sutskever. Deep double descent: Where bigger models and more data hurt. *arXiv preprint arXiv:1912.02292*, 2019.

[65] Stephen Casper, Xavier Boix, Vanessa D'Amario, Ling Guo, Kasper Vinken, and Gabriel Kreiman. Removable and/or repeated units emerge in overparametrized deep neural networks. *arXiv preprint arXiv:1912.04783*, 2019.

[66] Adam Kortylewski, Bernhard Egger, Andreas Schneider, Thomas Gerig, Andreas Morel-Forster, and Thomas Vetter. Empirically analyzing the effect of dataset biases on deep face recognition systems. In *Proceedings of the IEEE Conference on Computer Vision and Pattern Recognition Workshops*, pages 2093–2102, 2018.

[67] Pascal Mueller, Simon Haegler, Andreas Ulmer, Matthias Schubiger, Stefan Müller Arisona, and Basil Weber. *Esri CityEngine - a 3D city modeling software for urban design, visual effects, and VR/AR*. Esri R&D Center Zurich, Accessed 2020. URL `http://www.esri.com/cityengine`.

[68] Blender Online Community. *Blender - a 3D modelling and rendering package*. Blender Foundation, Stichting Blender Foundation, Amsterdam, Accessed 2020. URL `http://www.blender.org`.

[69] Antonio Torralba and Alexei A Efros. Unbiased look at dataset bias. In *Proceedings of the IEEE Conference on Computer Vision and Pattern Recognition (CVPR)*, pages 1521–1528, 2011.

[70] Diederik P Kingma and Jimmy Ba. Adam: A method for stochastic optimization. *arXiv preprint arXiv:1412.6980*, 2014.

A Additional details on Datasets (Section 2)

A.1 Samples from MNIST-Position and MNIST-Scale datasets

Fig. A.7 presents one representative example for each category-pose combination through the *combinations grid* for the MNIST-Position and MNIST-Scale datasets.

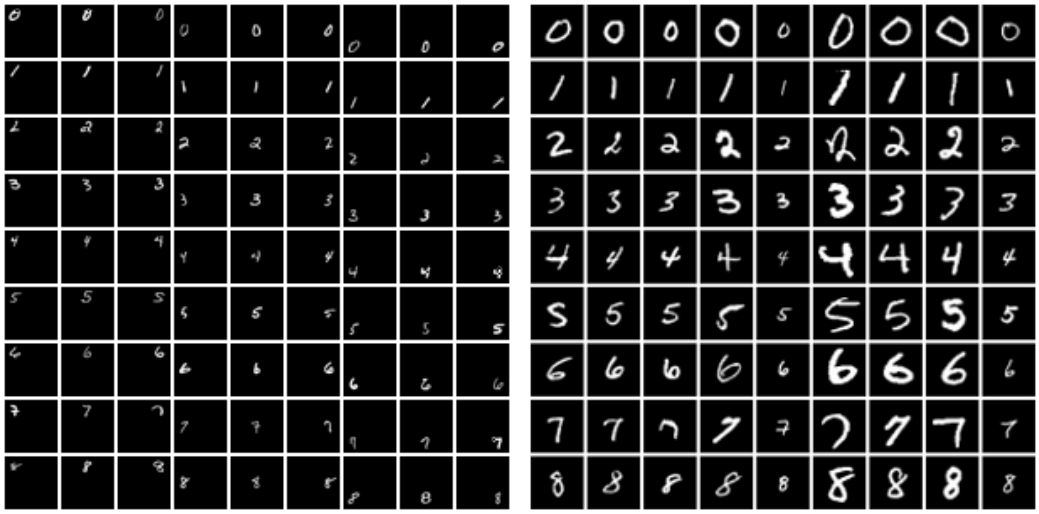

(a) MNIST-Position (b) MNIST-Scale

Figure A.7: *Combinations grids for MNIST-Position and MNIST-Scale.* Each row represents images from a category and each column from a pose. (a) MNIST-Position was created by adding pose in the form of position to images. For this, MNIST images were placed into one of nine positions in an empty three-by-three grid with equal probability. (b) MNIST-Scale was created by resizing images from MNIST to one of nine possible sizes, and then zero-padding.

A.2 Rendering Pipeline for *Biased-Cars* Dataset

To generate photo-realistic data with systematic, controlled biases we implemented our computer graphics pipeline which offered us fine grained control over scene attributes including but not limited to - backgrounds, textures, lighting and geometry. Below we present the details of our rendering pipeline, along with some sample images.

Pipeline Details: We used Esri CityEngine [67] to model the city layout and geometry, to which we add 3D assets - car models, pedestrians, trees, street furniture like bus stops, textures for buildings, roads and car paints. Blender Python API [68] is used to modify the 3D city file. This includes placing vehicles and other assets at user defined locations, modifying their material properties including vehicle paint, adding specified textures to roads, buildings and pedestrians, and defining camera attributes (lens, field of view, motion blur etc) and camera locations. For randomization, a distribution over each parameters was defined. For instance, a discrete uniform distribution over possible car color paints. Similarly, we defined distributions over object positions in the city, camera viewpoint and distance, among other factors.

Sample images are shown in Fig. A.8 below, rendered at 1024×1024 pixels. As network input was 224×224, training images were rendered at 256×256 and then resized to 224×224 (as side length of the form 2^k lead to computational gains in physically based rendering). Physically based rendering accurately models the flow of light in the scene resulting in highly photo-realistic images. As can be seen, our pipeline reproduces lighting artefacts like color bleeding and specular highlights very gracefully. As shown, images include cars seen from different distances and viewpoints, under different lighting conditions, scene clutter and even occlusions.

Figure A.8: *Sample images from the Biased-Cars dataset.*

B Experimental Details and Hyper-Parameters (Section 3)

Each of our four datasets contains both category and pose labels for all images. We define the location and the scale as the pose for MNIST-Position and MNIST-Scale datasets respectively. For both iLab and *Biased-Cars* dataset, the pose refers to the azimuth viewpoint. Networks are trained to predict both category and pose labels simultaneously, and all models are trained from scratch, without any pre-training to ensure controlled testing. This ensures that any existing biases in common pre-training datasets like ImageNet [69] do not impact our results.

Number of Images: The number of training images is kept fixed for every dataset, and was decided by training networks on these datasets while gradually increasing size, till the performance on *unseen* combinations saturated. For the *Biased-Cars* dataset, performance plateaud at 3,400 train, 445 validation, and 800 *unseen* test images. For iLab, we used 70,000 train, 8,000 validation images, and 8,000 *unseen* test images. As the iLab dataset is a natural image dataset, it required much more images to saturate. For MNIST, 54,000 train, 8,000 validation and 8,000 test images were used.

Hyper-parameters: We used the Adam [70] optimizer with 0.001 as learning rate, and ReLU activations. For the *Biased-Cars* datasets, all models were trained for 200 epochs, while we trained for 50 epochs for the iLab dataset. MNIST-Position and MNIST-Scale were trained for 5 epochs. These stopping criterion were picked to ensure convergence on generalization to *unseen* combinations. All experiments were repeated multiple times and confidence intervals are shown in the plots in the main paper. iLab and *Biased-Cars* experiments were repeated 3 times each, and MNIST experiments were repeated 10 times. Loss for training *Shared* architectures was simply the sum of CrossEntropy Loss for both category and Pose prediction. We compared how different weighted sums perform, and found this to be performing best as measured by the geometric mean of category and pose prediction.

C Selectivity and Invariance (Section 4)

In the paper we defined the selectivity score of a neuron with respect to category and its invariance score with respect to pose. Following the same notation as the paper: a^k_{ij} denotes the *activations grid* for neuron k, where each row represents one category and each column represents a pose.

C.1 Normalization of *activations grid*

For every neuron, we first normalize its activations for every image by dividing them by its maximum activation across all images. This ensures that that the activation for every image lies between 0 and 1 for all neurons. The entries of the *activations grid* for a neuron are then computed by averaging these normalized activation for images belonging to each category-pose combination.

The *activations grid* is then normalized to be between 0 and 1. To do so, we subtract the minimum of the *activations grid* and then divide it by the maximum.

C.2 Selectivity and Invariance with respect to Pose

In the paper, we used $i^{\star k}$, S^k_c, I^k_p to denote the *preferred category*, selectivity score with respect to category and invariance score with respect to pose respectively. We also presented these equations to compute these quantities:

$$i^{\star k} = \arg\max_i \sum_j a^k_{ij}. \tag{C.4}$$

$$S^k_c = \frac{\hat{a}^k - \bar{a}^k}{\hat{a}^k + \bar{a}^k}, \quad \text{where } \hat{a}^k = \frac{1}{N}\sum_j a^k_{i^{\star k}j}, \;\; \bar{a}^k = \frac{\sum_{i \neq i^{\star k}} \sum_j a^k_{ij}}{N(N-1)}. \tag{C.5}$$

$$I^k_p = 1 - \left(\max_j \; a^k_{i^{\star k}j} - \min_j \; a^k_{i^{\star k}j}\right) \tag{C.6}$$

We now present how to compute the selectivity with respect to pose, and invariance with respect to category, denoted as S_p^k and I_c^k respectively. These can be obtained by first finding the *preferred pose*, denoted as $j^{\star k}$, and proceeding as in the above equations:

$$j^{\star k} = \arg\max_j \sum_i a_{ij}^k. \tag{C.7}$$

$$S_p^k = \frac{\hat{a}^k - \bar{a}^k}{\hat{a}^k + \bar{a}^k}, \quad \text{where } \hat{a}^k = \frac{1}{N}\sum_i a_{ij^{\star k}}^k, \;\; \bar{a}^k = \frac{\sum_{j \neq j^{\star k}} \sum_i a_{ij}^k}{N(N-1)}. \tag{C.8}$$

$$I_c^k = 1 - \left(\max_i \; a_{ij^{\star k}}^k - \min_i \; a_{ij^{\star k}}^k\right) \tag{C.9}$$

Observe that like S_c^k, S_p^k is a value between 0 and 1, and higher value indicates that the neuron is more active for the *preferred pose* as compared to the rest of the poses. I_c^k too is a value between 0 and 1, with higher values indicating higher invariance to the category for images containing the *preferred pose*.

D Additional Results for Section 5

Below we present additional results that re-inforce our findings presented in Section 5 of the main paper.

D.1 Number of Training examples

To ensure that our findings are not a function of the amount of training data, we present the results for different number of images for the *Biased-Cars* and the iLab dataset in Fig. D.9. As can be seen in both these datasets, across a different number of images the *Separate* architecture substantially outperforms the *Shared* one at generalizing to *unseen* category-pose combinations.

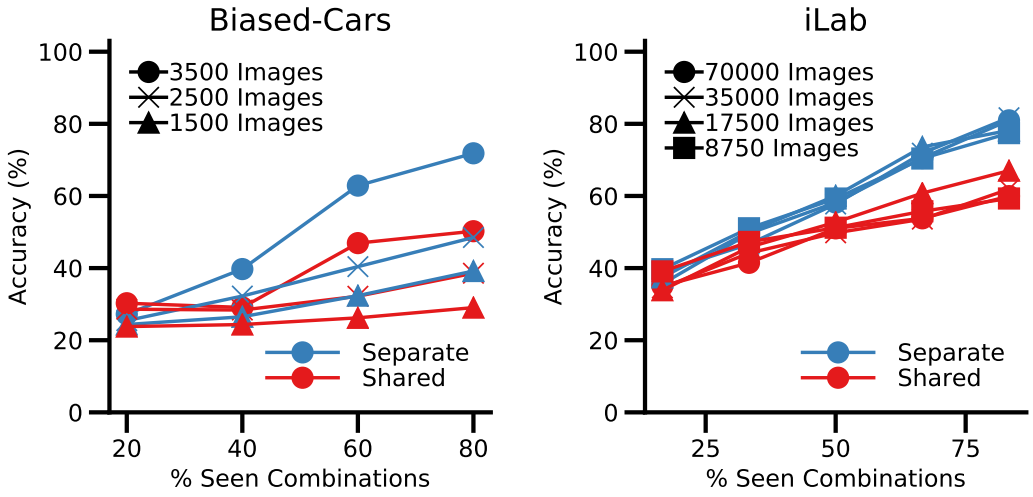

Figure D.9: *Generalization to unseen combinations as number of training images is varied.* For both iLab and Biased-Cars dataset, *Separate* architecture outperforms the *Shared* architecture trained with the same number of images.

D.2 Number of neurons in shared *vs.* separate networks

To control for the number of neurons in *Shared* and *Separate* architectures, we present additional results with the *Biased-Cars* dataset in Fig. D.10. In the paper, we presented the *Shared-Wide*

architecture for the ResNet-18 backbone, which is the *Shared* architecture with double the number of neurons per layer, *ie.,* double the width. Here we go one step further and test a number of similar scenarios with the ResNet-18 backbone. The *Separate Half* and *Separete One Fourth* architectures are made by reducing the number of neurons in every layer to one half, and one fourth of the original number respectively. It is to be noted, that the *Separate* architectures has double the number of neurons as the *Shared* architecture, as there is no weight sharing between branches in the *Separate* case. Thus, the *Separate Half* architecture has the same number of neurons as the *Shared* architecture, and the *Separate* architecture has the same number as the *Shared-Wide* architecture. In a similar vein, the *Shared Four Times* was created by multiplying the neurons in each layer of the *Shared* architecture four times. Thus, the *Shared Four Times* has double the number of neurons as compared to the *Shared Wide* architecture, and 4 times the *Shared* architecture.

As can be seen in Fig. D.10, even at one-eighth number of neurons, the *Separate One Fourth* architecture substantially outperforms the *Shared Four Times* architecture at generalizing to *unseen* category-pose combinations. This confirms that our findings are not a function of the number of neurons in the *Shared* and *Separate* architectures.

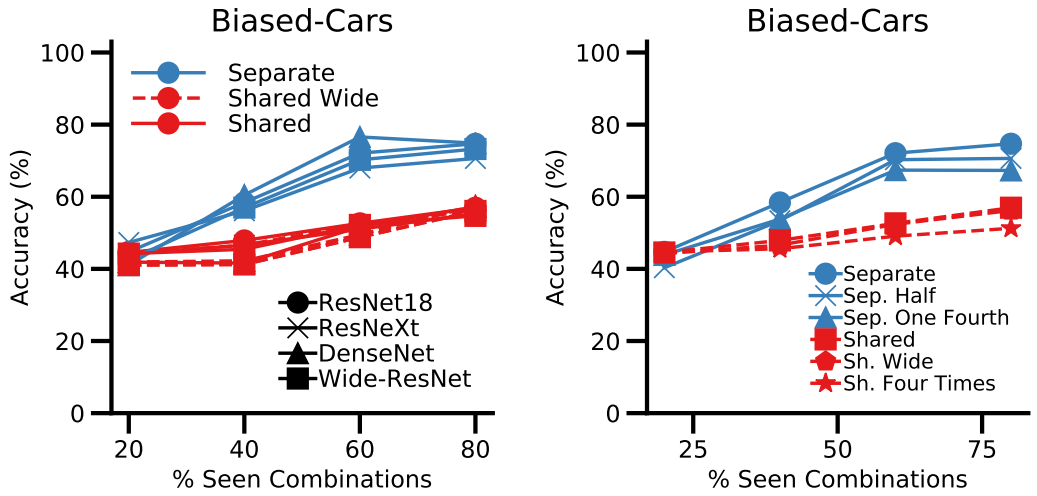

Figure D.10: *Generalization to unseen combinations as number of neurons per layer are varied for the ResNet-18 backbone. Separate* architectures substantially outperform *Shared* architectures across a range of widths, *ie.,* number of neurons per layer. The *Separate* architecture contains double the parameters as the *Shared* architecture, as there is no weight sharing in the *Separate* case. Variants of these architectures are created by increasing or decreasing the neurons in each layer by a factor of 2 at a time. Even at one-eighth the number of neurons, the *Separate One Fourth* architecture generalizes much better to unseen combinations as compared to the *Shared Four Times* architecture.

D.3 Separate performance of Category and Pose prediction

In Fig. E.12, we show that accuracy for category and pose prediction in *unseen* category-pose combinations. The results show that *Separate* also obtains better accuracy than *Shared* for each individual task accuracy. Note that depending on the dataset, category or pose predictions have different degrees of difficulty and not always category recognition is more difficult than pose estimation.

Furthermore, we have found that for MNIST-Position, the pooling operation at the end of ResNet-18 is critical to obtain good generalization accuracy to *unseen* category-pose combinations. We evaluated ResNet-18 without the pooling operation and the category recognition accuracy of *unseen* category-pose combinations dropped to baseline. Pooling facilitates an increase of position invariance and it does not harm the pose estimation accuracy (as shown by [27], pooling does not remove the position information).

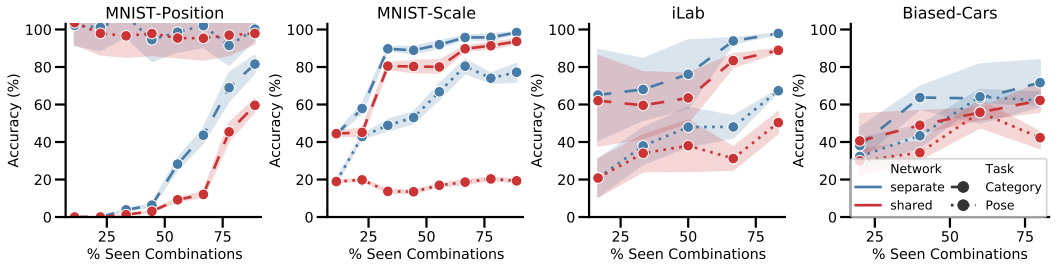

(a) (b) (c) (d)

Figure D.11: *Generalization performance for Shared and Separate ResNet-18 as seen combinations are increased for all datasets.* The category recognition accuracy and pose estimation accuracy are reported along with confidence intervals (a) MNIST-Position dataset. (b) MNIST-Scale dataset. (c) iLab dataset. (d) Biased-Cars dataset.

E Additional Results for Section 6

E.1 Specialization for other datasets

In the main paper we have presented specialization scores for the iLab and *Biased-Cars* dataset. Here we also provide these for the MNIST-Position and MNIST-Scale datasets. As can be seen, our findings are consistent across these datasets as well. Fig E.12a and b show that neurons in the final convolutional layer specialize to become either category or pose neurons as more category-pose combinations are shown. Category and pose branches of the *Separate* architecture become completely specialized to category and pose respectively. In the *Shared* architecture, both kinds of neurons emerge in roughly equal numbers. Fig E.12c and d show that as the number of *seen* combinations are increased, there is a steady increase in the specialization score for both MNIST-Position and MNIST-Scale.

In Fig. E.13, we show that the selectivity score results are also consistent in iLab for different backbones and split architectures.

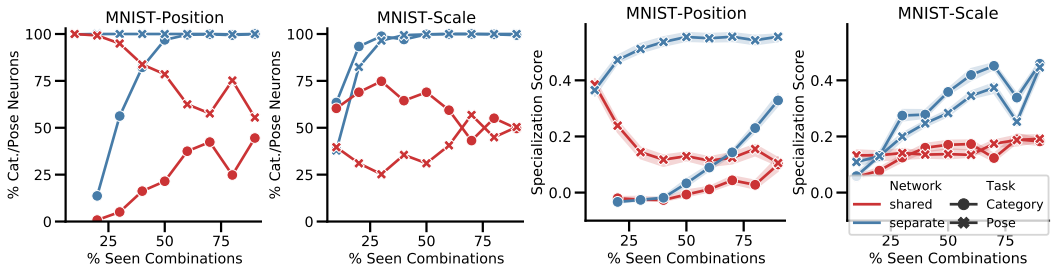

(a) (b) (c) (d)

Figure E.12: *Neuron specialization in MNIST-Position and MNIST-Scale datasets*. (a) and (b) Percentage of neurons in the final convolutional layer of ResNet-18 that are specialized to category and pose, for MNIST-Position and MNIST-Scale datasets, respectively. (c) and (d) Median of the specialization scores of neurons in the final convolutional layer of ResNet-18 *Separate* and *Shared* architectures, for category and pose recognition tasks, respectively.

E.2 Invariance and Selectivity Scores

In Fig. E.14 and E.15, we show the invariance and selectivity scores separately for the *Biased-Cars* dataset. In both cases, the trends follow what we observed for the specialization score, though the differences are much more pronounced in terms of invariance rather than selectivity.

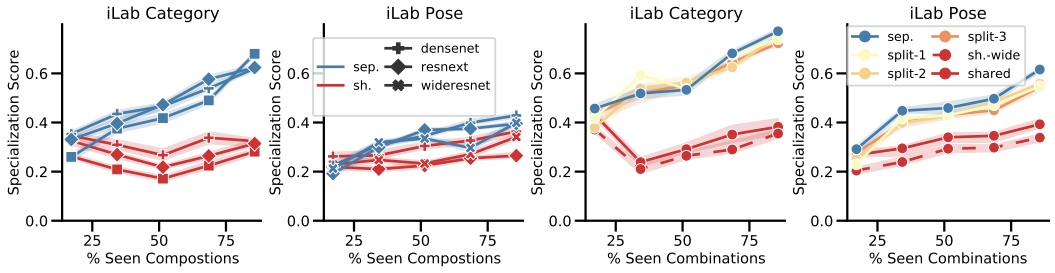

Figure E.13: *Neuron specialization (selectivity to category and invariance to pose, and vice versa) in the iLab dataset.* (a) and (b) Median of the specialization score among neurons (Γ^k) in network architectures, other than ResNet-18, *separate* and *shared*, for category and pose recognition tasks, respectively. Confidence intervals displayed in low opacity. (c) and (d) Median of the specialization score among neurons in ResNet-18 *Separate* and *Shared* with splits made at different blocks of the network, for category and pose recognition tasks, respectively. Similar results for the *Biased-Cars* dataset are provided in the main paper.

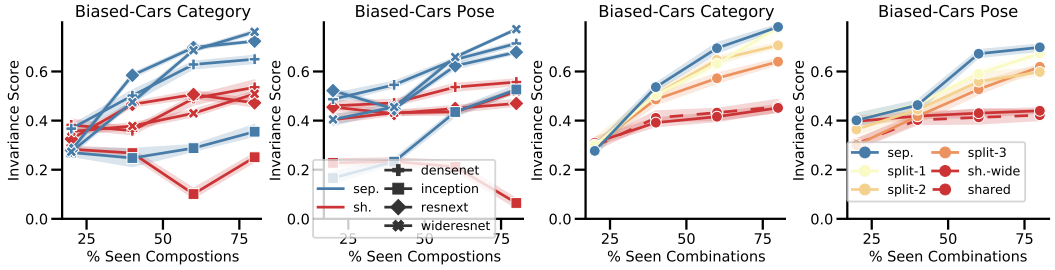

Figure E.14: *Invariance scores in the Biased-Cars dataset.* (a) and (b) Median of the invariance score among neurons in network architectures, other than ResNet-18, *separate* and *shared*, for category and pose recognition tasks, respectively. Confidence intervals displayed in low opacity. (c) and (d) Median of the invariance score among neurons in ResNet-18 *Separate* and *Shared* with splits made at different blocks of the network, for category and pose recognition tasks, respectively.

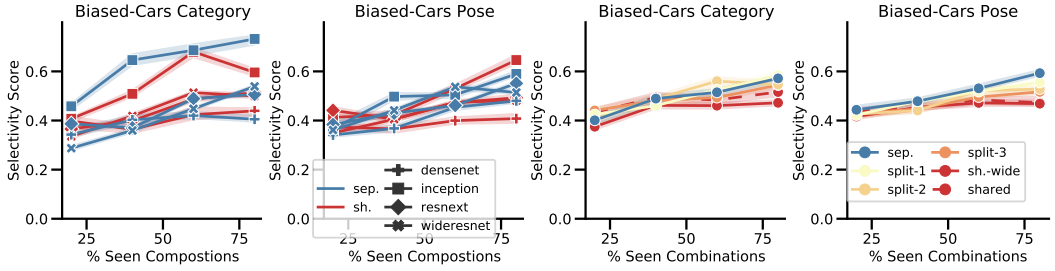

Figure E.15: *Selectivity scores in the Biased-Cars dataset.* (a) and (b) Median of the selectivity score among neurons in network architectures, other than ResNet-18, *separate* and *shared*, for category and pose recognition tasks, respectively. Confidence intervals displayed in low opacity. (c) and (d) Median of the selectivity score among neurons in ResNet-18 *Separate* and *Shared* with splits made at different blocks of the network, for category and pose recognition tasks, respectively.

E.3 Specialization Score per Layer

In Fig. E.16, we show the specialization score in each layer. We can see that it builds up across layers, and this is more pronounced for *Separate* architectures than for *Shared*.

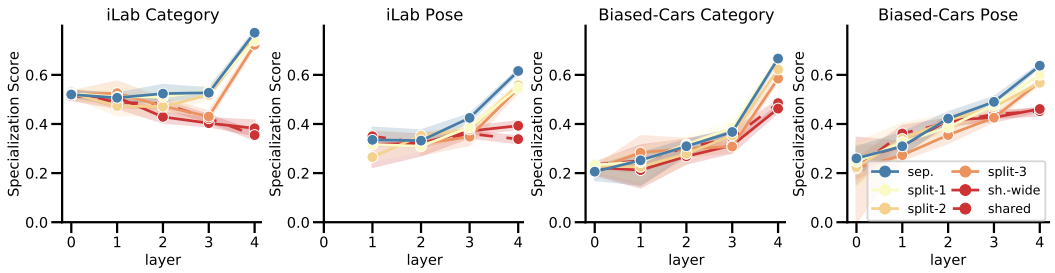

(a) (b) (c) (d)

Figure E.16: *Specialization Score Per Layer for* 30 seen *category-pose Combinations for iLab, and* 20 seen *category-pose Combinations for the Biased-Cars dataset.* (a) and (b) Median of the specialization score among neurons in ResNet-18 *Separate* and *Shared* with splits made at different blocks of the network, for category and pose recognition tasks, respectively. (c) and (d) Same as (a) and (b) for *Biased-Cars* dataset.